nature neuroscience

ARTICLES

https://doi.org/10.1038/s41593-021-00843-3

Check for updates

CaMKII activation persistently segregates postsynaptic proteins via liquid phase separation

Tomohisa Hosokawa[1,2,3,8], Pin-Wu Liu[1,8], Qixu Cai[4], Joana S. Ferreira[5], Florian Levet[5], Corey Butler[5], Jean-Baptiste Sibarita[5], Daniel Choquet[5,6], Laurent Groc[5], Eric Hosy[5], Mingjie Zhang[4,7] ✉ and Yasunori Hayashi[1] ✉

Transient information input to the brain leads to persistent changes in synaptic circuits, contributing to the formation of memory engrams. Pre- and postsynaptic structures undergo coordinated functional and structural changes during this process, but how such changes are achieved by their component molecules remains largely unknown. We found that activated CaMKII, a central player of synaptic plasticity, undergoes liquid–liquid phase separation with the NMDA-type glutamate receptor subunit GluN2B. Due to CaMKII autophosphorylation, the condensate stably persists even after Ca^{2+} is removed. The selective binding of activated CaMKII with GluN2B cosegregates AMPA receptors and the synaptic adhesion molecule neuroligin into a phase-in-phase assembly. In this way, Ca^{2+}-induced liquid–liquid phase separation of CaMKII has the potential to act as an activity-dependent mechanism to crosslink postsynaptic proteins, which may serve as a platform for synaptic reorganization associated with synaptic plasticity.

Inside a central excitatory synapse, various molecules are segregated into functional nanodomains to accomplish the intricate regulation of synaptic transmission and plasticity. In the presynaptic compartment, the readily releasable pool of vesicles is concentrated at specialized nanodomains referred to as active zones. On the postsynaptic membrane, different classes of glutamate receptor form discrete nanodomains[1–4]. These pre- and postsynaptic nanodomains are matched with each other, forming trans-synaptic nanocolumns or nanomodules that ensure an efficient transmission between pre- and postsynaptic structures[1,2,5,6].

However, how such nanodomains are formed and regulated by neuronal activity in the absence of any demarcating membranous structures has not been fully elucidated. Recently, liquid–liquid phase separation (LLPS) of biological macromolecules was found to play a critical role in regulating the assembly and segregation of molecules in various intracellular structures[7,8]. In this regard, Ca^{2+}/calmodulin-dependent protein kinase II (CaMKII)—a highly abundant protein kinase in the postsynaptic density (PSD)—has ideal features to undergo LLPS[7,8]. Ca^{2+}/calmodulin binding to CaMKII opens up a binding pocket called the T-site, which is occupied by the autoinhibitory domain encompassing threonine (T) 286 in inactive kinase, and forms a stable complex, at micromolar affinity, with various synaptic proteins, such as the carboxyl tail of NMDA-type glutamate receptor (NMDAR) subunit GluN2B (Supplementary Fig. 1) and RacGEF protein Tiam1 (refs. [9,10]). Once bound, it persists even when the cellular Ca^{2+} concentration decreases[9,10]. Finally, the dodecameric structure of CaMKII[11] allows multivalent interactions.

Given this, we explored whether CaMKII has the ability to undergo LLPS with PSD proteins and, if it does, how it can affect synaptic protein distribution and function. We found that Ca^{2+} activation of CaMKII results in persistent LLPS with PSD proteins in a manner requiring T286 autophosphorylation. CaMKII then segregates two subtypes of glutamate receptor, AMPAR and NMDAR, through the formation of phase-in-phase, which was recapitulated in neurons as shown by super-resolution microscopy. Neuroligin-1 (NLGN1), a neuronal adhesion molecule, which clusters presynaptic neurexin and other active zone proteins, segregates together with AMPAR. From these observations, we propose that the persistent LLPS of activated CaMKII serves as an activity-dependent mechanism to crosslink proteins beneath postsynaptic membrane. This may also align the AMPAR nanodomain with the presynaptic transmitter release site, thereby serving as a previously unknown mechanism of synaptic plasticity.

Results

CaMKII undergoes LLPS with GluN2B carboxyl tail. To test the idea that CaMKII can undergo LLPS with its T-site binding partner, we combined purified CaMKII with the carboxyl tail of GluN2B, a prototypical T-site binding protein (residues 1226–1482, GluN2Bc). GluN2Bc was fused with dimeric near-infrared fluorescent protein eqFP670 to label it and to mimic the subunit stoichiometry of the GluN2B subunit in the endogenous NMDAR complex. We used a low-speed centrifugation assay to assess macromolecular complex formation[12–14]. The cytoplasmic concentration of CaMKII in the synapse is estimated to be 20–80 μM as a monomer[15]. Here, we used 10 μM of CaMKII as this was the practical limit of the preparation. Generally, proteins form condensates more readily at higher concentration. Therefore, we are towards the more conservative side in making this conclusion. On the other hand, GluN2B is a membrane protein and it is difficult to define its concentration/density. Also, association with the membrane limits the diffusion and stability of GluN2B, which can effectively increase the valency of the

[1]Department of Pharmacology, Kyoto University Graduate School of Medicine, Kyoto, Japan. [2]RIKEN Brain Science Institute, Saitama, Japan. [3]Department of Molecular Biology, Division of Biological Science, Nagoya University Graduate School of Science, Nagoya, Japan. [4]Division of Life Science, Hong Kong University of Science and Technology, Kowloon, Hong Kong, China. [5]Université de Bordeaux, Interdisciplinary Institute for Neuroscience, UMR 5297, Bordeaux, France. [6]Bordeaux Imaging Center, Bordeaux, France. [7]School of Life Sciences, Southern University of Science and Technology, Shenzhen, China. [8]These authors contributed equally: Tomohisa Hosokawa, Pin-Wu Liu. ✉e-mail: mzhang@ust.hk; yhayashi-tky@umin.ac.jp

interaction. Therefore, we tentatively used GluN2B at the same concentration as CaMKII. When CaMKII, GluN2Bc and calmodulin were mixed in the absence of Ca^{2+}, the proteins stayed in the supernatant (Fig. 1a,b). However, upon addition of Ca^{2+}, most CaMKII moved to the pellet with GluN2Bc, indicating that Ca^{2+} stimulation of CaMKII induces the formation of a macromolecular complex with GluN2Bc. Differential interference contrast (DIC) and fluorescent microscopy showed no condensate in the absence of Ca^{2+} (Fig. 1c). However, the addition of Ca^{2+} induced formation of protein condensates containing CaMKII and GluN2Bc, consistent with the sedimentation assay[12,14]. Upon point photobleaching in a single condensate, both CaMKII and GluN2Bc fluorescence recovered after photobleaching (Fig. 1d and Supplementary Fig. 2). Once formed, the condensates were stable, and we could observe two droplets fusing together to form a larger droplet (Fig. 1e). These observations indicate that the condensate retained liquid-like properties. GluN2Bc without CaMKII, or with CaMKII with eqFP670 fusion tag only, did not pellet or form condensates, indicating that both CaMKII and GluN2Bc are required (Supplementary Fig. 3a–d). The carboxyl tails of AMPA receptor subunits GluA1 and GluA2 did not form condensates with CaMKII (Supplementary Fig. 3e). Together, our results indicate that Ca^{2+}/calmodulin can trigger formation of protein condensates containing CaMKII and GluN2Bc by a LLPS-mediated mechanism.

Autophosphorylation of CaMKII is required for persistence of protein condensate. CaMKII and GluN2Bc protein condensates persisted even after the addition of ethylene glycol tetra-acetic acid (EGTA), a Ca^{2+}-chelator (Fig. 1a–c). In contrast, in the absence of ATP, condensates could form but dissolved upon addition of EGTA (Fig. 1b,f and Supplementary Fig. 4a). This indicates that the kinase reaction is involved in the persistence of condensates after Ca^{2+} dissipates. All experiments described hereafter were performed in the presence of ATP unless otherwise indicated. Consistent with the experiment in the absence of ATP, a kinase null CaMKII K42R mutant formed condensates in the presence of Ca^{2+} but failed to persist after the addition of EGTA (Fig. 1g). Mutation of the autophosphorylation site at T286, a site required for the constitutive activation of CaMKII beyond the period of elevated Ca^{2+} concentration, to alanine (T286A) replicated the results of the kinase null mutant (Fig. 1h). These results indicate that autophosphorylation at T286 is not critical for the initial formation of condensates by Ca^{2+} but is required for the persistent maintenance of the condensates in the absence of Ca^{2+}.

We next tested if the multivalent interaction between CaMKII and GluN2Bc is required for the formation of condensates. Consistent with the requirement of multivalency of CaMKII, a catalytically active but monomeric CaMKII mutant 1–314 lacking the association domain failed to form condensates (Supplementary Fig. 4b). To prevent the specific interaction between CaMKII and GluN2Bc, we turned to a model of binding between CaMKII and GluN2B (ref. [16]). The model shows the interaction between a hydrophobic pocket made by I205 and F98 of CaMKII with L1298 of GluN2B as well as electrostatic interactions between E139 of CaMKII and R1300 of GluN2B. A CaMKII T-site mutant I205K failed to form condensates (Supplementary Fig. 4c). Also, GluN2Bc mutants that cannot interact with CaMKII, L1298A/R1300Q (LR/AQ) and R1300Q/S1303D (RS/QD) (refs.[9,17]) failed to form condensates (Supplementary Fig. 4d,e). These results indicate that multivalent interactions via those hydrophobic and electrostatic interactions between the CaMKII T-site and GluN2Bc are required for the formation of condensates.

To obtain temporal information on the formation and dispersion of condensates, we measured the turbidity of the protein mixture (Supplementary Fig. 5) (ref. [18]). The turbidity of the CaMKII/GluN2Bc sample increased within 30 s of the addition of Ca^{2+}, and remained after adding EGTA. On the other hand, the turbidity of the T286A/GluN2Bc sample increased similarly to the wildtype CaMKII sample but decreased to baseline amounts within 30 s of EGTA treatment.

Segregation of AMPAR and NMDAR by a CaMKII LLPS-mediated mechanism. We then added further components of the PSD to examine if CaMKII can form condensates with other main PSD proteins as well. We tested the carboxyl tail of Stargazin (STGc), an auxiliary subunit of AMPAR critical for determining its synaptic distribution, as a proxy of the AMPA receptor, and PSD-95, which can interact with both GluN2Bc and STGc through PDZ domains[13,19,20] (Supplementary Fig. 1). STGc was fused with a tetrameric fluorescent protein DsRed2 to mimic the stoichiometry of the endogenous AMPAR complex. When CaMKII, calmodulin, PSD-95, GluN2Bc and STGc were combined, PSD-95, GluN2Bc and STGc formed homogenous condensates while CaMKII remained in the more dilute phase in the absence of Ca^{2+} (Fig. 2a–c)[20]. However, when Ca^{2+} was added, CaMKII partitioned into the condensates, which persisted after the addition of EGTA. Intriguingly, we found segregation of proteins in the condensate. CaMKII and GluN2Bc came to the periphery and surrounded PSD-95 and STGc, which formed a phase-in-phase organization (Fig. 2c). Z-axis reconstruction showed that CaMKII and GluN2Bc entirely covered PSD-95 and STGc (Fig. 2d). While STGc was exclusively enriched in the inner phase, PSD-95 was partitioned in the peripheral phase as well (Fig. 2e). Conversely, both CaMKII and GluN2Bc were also partly partitioned in the inner phase. Again, consistent with liquid-like properties, we observed condensates fusing with each other (Fig. 2f).

Formation of the phase-in-phase organization requires CaMKII. Without CaMKII, Ca^{2+} failed to induce phase-in-phase assembly (Supplementary Fig. 6a). In the presence of CaMKII, phase-in-phase assembly could be induced in the absence of ATP (Supplementary Fig. 6b). However, after addition of EGTA, CaMKII moved to the more dilute phase and the condensates became homogenous (Supplementary Fig. 4b). Essentially the same results were obtained by using the CaMKII K42R (Supplementary Fig. 6c) and T286A (Supplementary Fig. 7a) mutants in the presence of ATP. These results indicate that neither kinase activity nor T286 phosphorylation is required for phase-in-phase assembly formation although GluN2B, Stg and PSD-95 are all known to be phosphorylated by CaMKII (ref. [9,19,20]). However, for the persistent phase-in-phase organization after the decrease in Ca^{2+} concentration, T286 autophosphorylation is crucial. CaMKII I205K and 1–314 mutants did not induce segregation (Supplementary Fig. 7b,c). Together, these results indicate that the segregation of GluN2Bc and STGc requires multivalent binding at the CaMKII T-site and GluN2Bc, but not the phosphorylation of any of the components. However, the persistent segregation after Ca^{2+} receding requires CaMKII T286 phosphorylation.

T-site interaction peptide can dissolve protein condensates. Different synaptic input patterns can induce bidirectional synaptic plasticity. We then wondered if there is any way to reverse the protein condensates. We turned to Camk2n1, a small endogenous CaMKII inhibitor protein that interacts with the T-site of CaMKII and is upregulated during memory processes[21]. Infusion of Camk2n1 to protein condensates resulted in collapse of the condensates (Fig. 3a,b and Supplementary Videos 1 and 2). In condensates composed of CaMKII/GluN2Bc/PSD-95/STGc, the surrounding CaMKII/GluN2Bc phase collapsed, while the PSD-95/STGc in the inner phase was more resistant, consistent with the fact that PSD-95/STGc by themselves form condensates[20] (Fig. 3b). To confirm that Camk2n1 disrupts the phase by competing with the T-site, we used CN21, a peptide derived from the minimum T-site binding region of Camk2n1 (ref. [22]). CN21, but not a scrambled peptide, collapsed the condensates formed by CaMKII and GluN2Bc

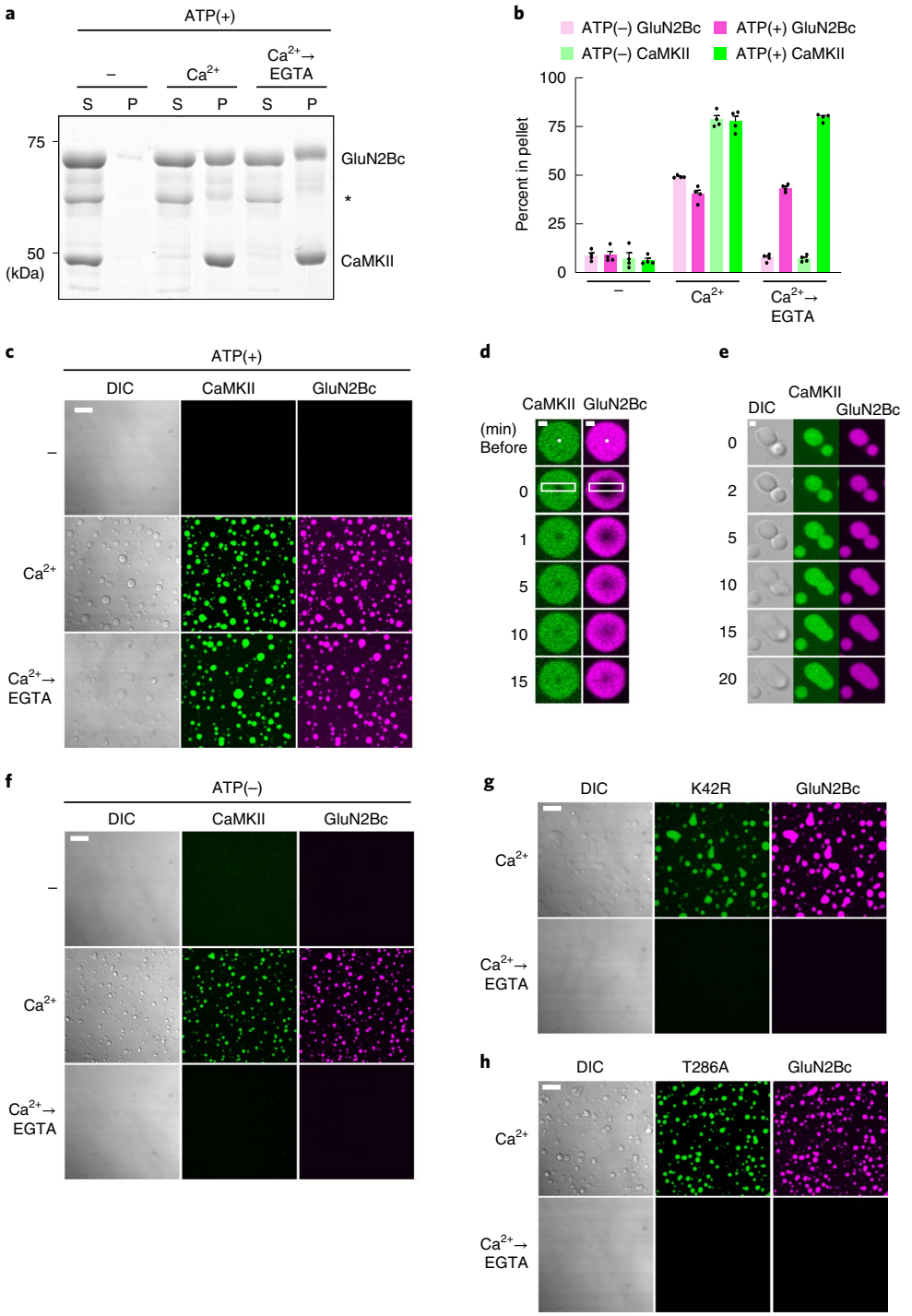

Fig. 1 | CaMKII and GluN2Bc form LLPS condensates. a, Low-speed sedimentation assay. CaMKII (10 μM) and GluN2Bc (10 μM) were mixed in the presence of 0.5 mM EGTA, 10 μM calmodulin, 5 mM $MgCl_2$ and 2.5 mM ATP (–). Then, 2 mM $CaCl_2$ (Ca^{2+}) was added, followed by 2.5 mM EGTA (Ca^{2+} → EGTA). The supernatant (S) and pellet (P) after centrifugation at 10,000*g* were subjected to SDS–PAGE and Coomassie brilliant blue staining. A slight upward shift of GluN2Bc is likely due to phosphorylation by CaMKII. The asterisk indicates a degradation product of GluN2Bc. Calmodulin is unobservable in the image due to its small size. An uncropped image of the gel is shown in Supplementary Fig. 13. **b**, Quantification of **a** (mean ± s.e.m.; $n = 4$ samples). **c**, DIC and confocal microscopic images of the protein mixture in **a**. CaMKII and GluN2Bc formed a condensate only in the presence of Ca^{2+}. Once formed, the condensate persisted even after the addition of EGTA. Scale bar, 10 μm. **d**, FRAP after photobleaching of a single point inside a condensate (indicated by white dot) of CaMKII–GluN2Bc in the presence of Ca^{2+}. Note that these are two separate experiments. Scale bar, 1 μm. See Supplementary Fig. 2 for quantification. **e**, A fusion event of condensates. Scale bar, 1 μm. **f**, Same experiment as in **c** in the absence of Mg^{2+}–ATP. Ca^{2+} triggers the formation of the condensate in the absence of Mg^{2+}–ATP. However, if EGTA is added, the condensate dispersed. Scale bar, 10 μm. **g**,**h**, Same experiment as in **c** using K42R (**g**) and T286A (**h**) mutants of CaMKII. Only Ca^{2+} and Ca^{2+} → EGTA conditions are shown. In both cases, the condensate formed in the presence of Ca^{2+} but did not persist after addition of EGTA. Combined, the results indicate that T286 phosphorylation is crucial for persistence of the condensate. Scale bar, 10 μm.

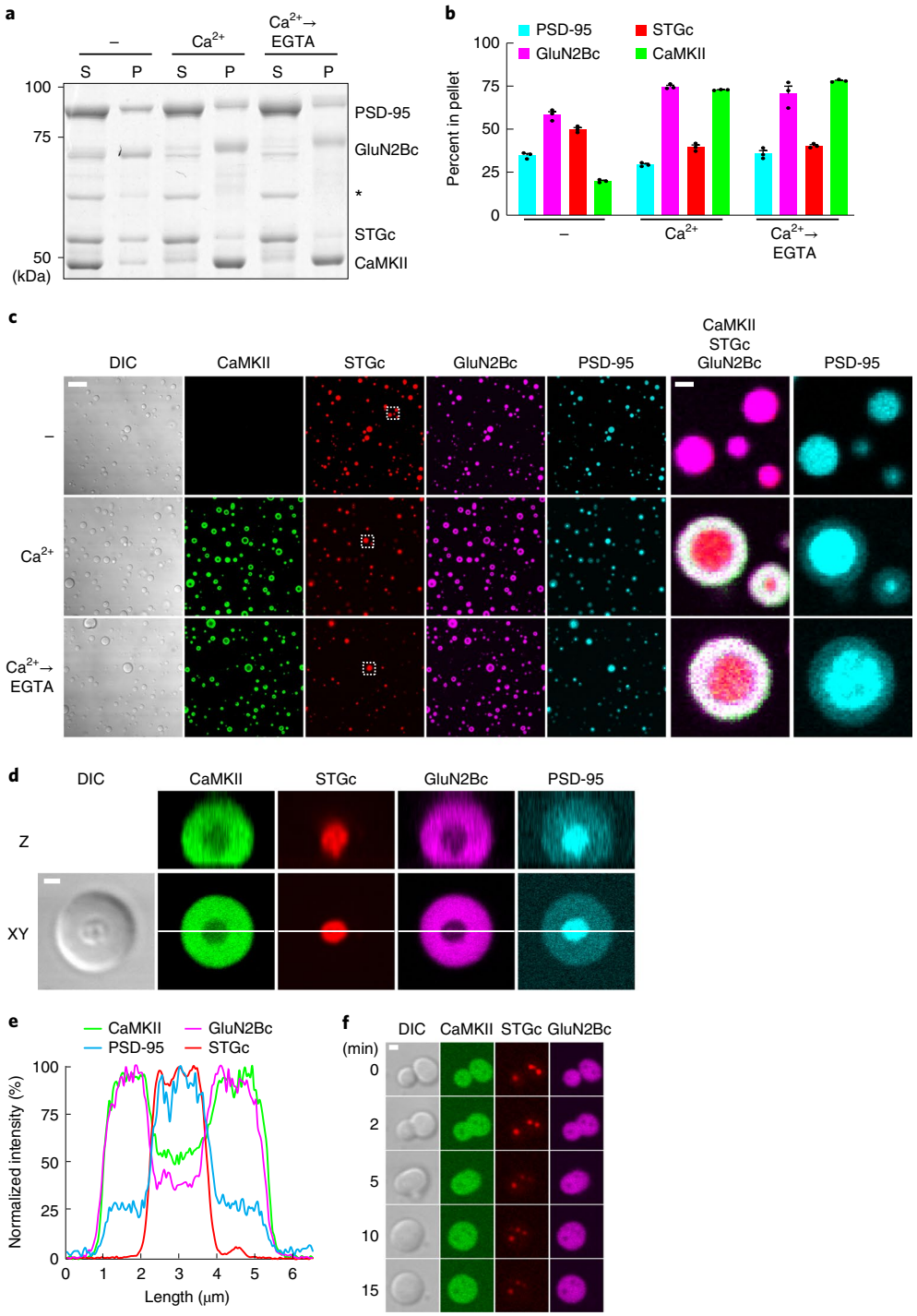

Fig. 2 | Segregation of AMPAR and NMDAR in protein condensate by active CaMKII. a, Sedimentation assay of 10 μM PSD-95, 2.5 μM GluN2Bc, 7.5 μM STGc, 10 μM CaMKII and 10 μM calmodulin in the presence of Mg^{2+}-ATP. The upward band shift and reduction in staining of PSD-95, GluN2Bc and STGc is likely due to phosphorylation by CaMKII. An uncropped image of the gel is shown in Supplementary Fig. 13. **b**, Quantification of **a** (mean ± s.e.m.; $n = 3$ samples). **c**, Images of the protein mixture in **a**. The two right-most columns are higher magnifications of the dashed rectangles in the STGc channel. Scale bars, 10 μm and 1 μm for low- and high-magnification images. **d**, Magnification and Z projection of single condensates. Scale bar, 1 μm. **e**, Line scanning of **d** in each color channel. **f**, Observation of a condensate fusion event. Scale bar, 1 μm. When stimulated with Ca^{2+}, PSD-95/STGc formed phase-in-phase while GluN2Bc/CaMKII formed a surrounding phase. This persisted even after addition of EGTA.

(Fig. 3c). Although CN21 is a CaMKII inhibitor, in this case, it does not affect existing phosphorylation as there is no phosphatase. These results indicate that the LLPS mediated by CaMKII can be reversed by Camk2n1 competition with GluN2Bc.

Tiam1 behaves as a Ca^{2+}-dependent client for CaMKII condensate. We then tested the possibility that other synaptic T-site proteins might serve as a client for the CaMKII/GluN2Bc condensate. We previously found that persistent binding between CaMKII

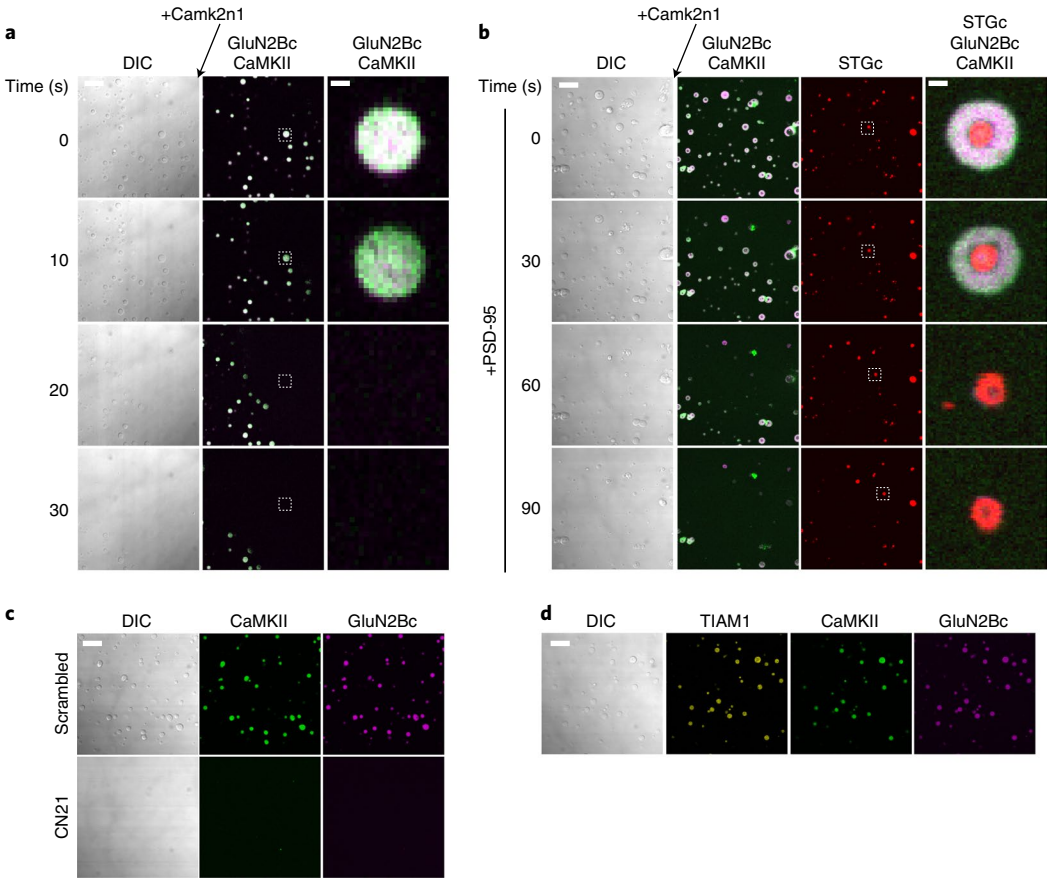

Fig. 3 | Dispersion of protein condensates by competing T-site interaction. a, Time-lapse imaging of CaMKII–GluN2Bc condensates (Ca^{2+} → EGTA condition) during infusion of 50 μM Camk2n1. The arrow shows the direction of infusion. See Supplementary Video 1. Scale bars, 10 μm and 1 μm for low- and high-magnification images, respectively. Note the complete dispersal of the condensate. **b**, Same experiment as in **a** using the condensates of CaMKII, GluN2Bc, PSD-95 and STGc. Due to the limited number of color channels available, PSD-95 was not imaged. See Supplementary Video 2. Note that the phase-in-phase of PSD-95/STGc was resistant to Camk2n1 application, indicating that these two proteins formed condensates by themselves. **c**, Effect of 5 μM scrambled and CN21 peptides for CaMKII/GluN2Bc condensates in Ca^{2+} → EGTA condition. CN21 replicated the effect of Camk2n1. **d**, Effect of 5 μM Tiam1 peptides for CaMKII/GluN2Bc condensates in Ca^{2+} → EGTA condition. Tiam1 peptide was taken up by the condensate without much affecting the LLPS. Scale bars, 10 μm and 1 μm for low- and high-magnification images, respectively.

and Tiam1, a RacGEF protein, after long-term potentiation (LTP) induction results in a reciprocally activating kinase-effector complex (RAKEC), which supports persistent Rac activity and the enlargement of dendritic spines[10]. We therefore tested if fluorescently labeled Tiam1 peptide corresponding to the CaMKII-binding domain (1544-DSHASRMAQLKKQAALSGINGG-1565) can be taken up by the protein condensate (Fig. 3d). We found that peptide was taken up by CaMKII/GluN2Bc condensates formed by the addition of Ca^{2+}. Once taken up, the peptide remained even after Ca^{2+} was chelated. This indicates that the protein condensate formed by CaMKII can serve as a mechanism to trap synaptic T-site binding proteins in an activity-dependent fashion.

Disruption of CaMKII T-site interaction decreases segregation between AMPAR and NMDAR. We then tested if CaMKII plays a role in segregating AMPAR and NMDAR in neurons by using direct stochastic optical reconstruction microscopy (dSTORM)[3,4]. We immunolabeled the endogenous AMPAR subunit GluA2 and NMDAR subunit GluN1 by using antibodies against their extracellular domains and then analyzed the overlap of synaptic nanodomains between the two receptor subtypes. In control neurons treated with cell-permeable peptide tat-scrambled (SCR), we observed that AMPAR and NMDAR formed distinct nanodomains (Fig. 4a). In neurons treated with tat-CN21 (CN21), the overlap was increased significantly compared with neurons treated with SCR, consistent with the idea that the segregation of AMPAR and NMDAR is dependent on CaMKII-mediated phase-in-phase assembly formation (Fig. 4b,c). The reason the proteins did not totally diffuse away upon CN21 treatment, unlike in the LLPS experiment, is likely due to the presence of several other mechanisms that still anchor the receptors at the synapse. We found no change in the area of nanodomain, the number of localization or the density of localization in CN21-treated neurons compared with neurons treated with SCR (Supplementary Fig. 8a–c).

NLGN cosegregates together with AMPAR. The trans-synaptic nanocolumn composed of presynaptic active zone and postsynaptic glutamate receptor is refined by neuronal activity, which can enhance the efficiency of synaptic transmission[2,5,23,24]. We wondered whether CaMKII-mediated segregation of postsynaptic proteins can communicate with the presynaptic terminal. We thus turned to examining the role of neuroligin-1 (NLGN), a neuronal adhesion molecule. NLGN interacts with presynaptic neurexin through its N-terminal extracellular domain, while the intracellular C-terminus interacts with the third PDZ domain (PDZ3) of PSD-95 (refs. [23,25–27]) (Supplementary Fig. 1). We fused the amino terminus of the intracellular carboxyl tail of NLGN (NLGNc) to the carboxyl terminus of dimeric Kusabira Green, a fluorescent

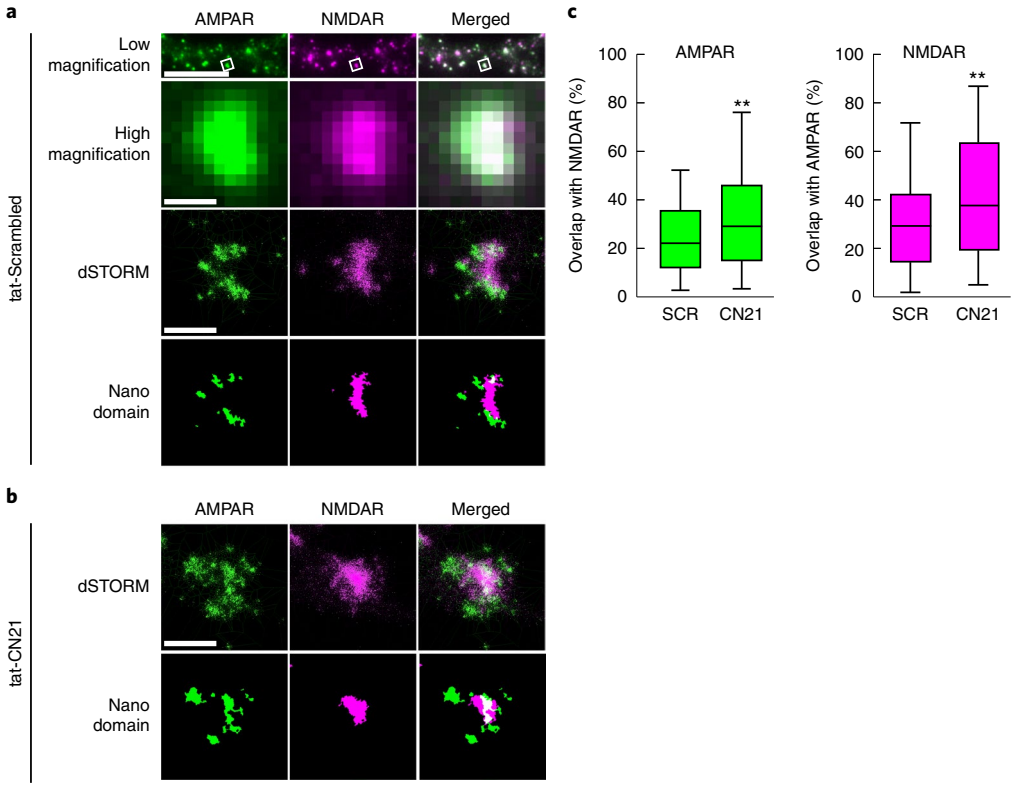

Fig. 4 | Reduction of synaptic glutamate receptor segregation by competing T-site interaction. a, Top row: low-magnification epifluorescence image of a dendrite from a hippocampal neuron in dissociate culture treated with 20 μM tat-scrambled peptide for 30 min and immunolabeled with anti-GluA2 (AMPAR, green) and anti-GluN1 (NMDAR, magenta). Scale bar, 10 μm. Second row: high-magnification image of a single synapse (in white squares in the low magnification image). Bottom two rows: dSTORM and thresholded images of the same region. Scale bar, 0.5 μm. **b**, Images of a synapse treated with 20 μM tat-CN21 for 30 min. **c**, Proportion of AMPAR nanodomains overlapping with NMDAR nanodomains (left, $P = 0.0098$) and of NMDAR nanodomains overlapping with AMPAR nanodomains (right, $P = 0.0019$) in tat-scrambled (SCR) or tat-CN21 (CN21) treated neurons. There was significantly more overlap in two receptor nanodomains in neurons treated with tat-CN21 than in those treated with tat-scrambled peptide. The dataset was obtained from 118 (SCR) and 116 (CN21) spines, from a total of 10 neurons for each treatment group. All neurons were processed in parallel using the same staining, acquisition and analysis parameters in blind fashion. The statistical significance of the results was assessed by two-sided Mann–Whitney *U* test. $^{**}P < 0.01$. The center line, the top and bottom of the box, and the whiskers of the blot indicate median, 25th–75th percentile and 5th–95th percentile, respectively.

protein, and tested if it could form condensates. NLGNc alone (not shown) or together with PSD-95 did not form condensates (Fig. 5a). Only when we added GluN2Bc or GluN2Bc and STGc, did NLGNc participate in condensates (Fig. 5a). Deletion of the PDZ domain binding motif of NLGNc (NLGNc-Δ7) excluded it from the condensates (Supplementary Fig. 9). These results indicate that NLGNc participates in PSD-95 condensates as a 'client' through its PDZ-binding motif. When we added CaMKII, before addition of Ca^{2+}, proteins other than CaMKII formed homogenous condensates (Fig. 5b with unlabeled CaMKII, Fig. 5c with unlabeled PSD-95). Upon stimulation with Ca^{2+}, NLGNc moved to the inner phase together with STGc/PSD-95, whereas GluN2Bc and CaMKII segregated to the outer phase (Fig. 5b,c and Supplementary Fig. 10). These results indicate that NLGN is partitioned together with AMPAR and forms a phase distinct from NMDAR, which might serve as a mechanism to position AMPAR beneath the presynaptic active zone. To test if the segregation of NMDAR and NLGN1 in neurons also depends on CaMKII, we treated the neurons in dissociated culture with tat-CN21 or tat-scrambled peptides, then surface-labeled and observed them by dSTORM (Supplementary Fig. 11). In neurons treated with tat-Scrambled peptide, NMDAR and NLGN1 were segregated from each other. In contrast, in neurons treated with tat-CN21, the segregation between them became significantly less.

Discussion

In this study, we showed that CaMKII can undergo LLPS with main PSD proteins, most notably GluN2B, through its multivalent interaction conferred by its dodecameric structure. This view is consistent with several properties of synaptic CaMKII, such as constant exchange at rest as shown by fluorescence recovery after photobleaching (FRAP) analysis[28], and rapid translocation to the synapse upon LTP induction in a manner requiring the interaction of CaMKII T-site with GluN2B carboxyl tail[17,29,30]. The formation of LLPS by CaMKII and GluN2B as well as Shank3 was reported as a separate article[31].

The initial formation of protein condensates was triggered by Ca^{2+} and was independent of kinase activity. Once formed, the condensate persisted even after the decrease in Ca^{2+} concentration. This persistence requires CaMKII T286 autophosphorylation, which maintains CaMKII in an open conformation and exposes the T-site[32], thereby allowing the binding of GluN2B. In its absence, the autoinhibitory domain docks at the T-site[11] and outcompetes binding with GluN2B. We speculate this is why T286 phosphorylation is required for the persistence of protein condensates. The size of protein condensate in the LLPS in vitro experiment is much larger than in a synapse. One reason for this difference may be due to the availability of the component molecules. In vitro, the amount of proteins is enormous compared to the situation in neurons, which

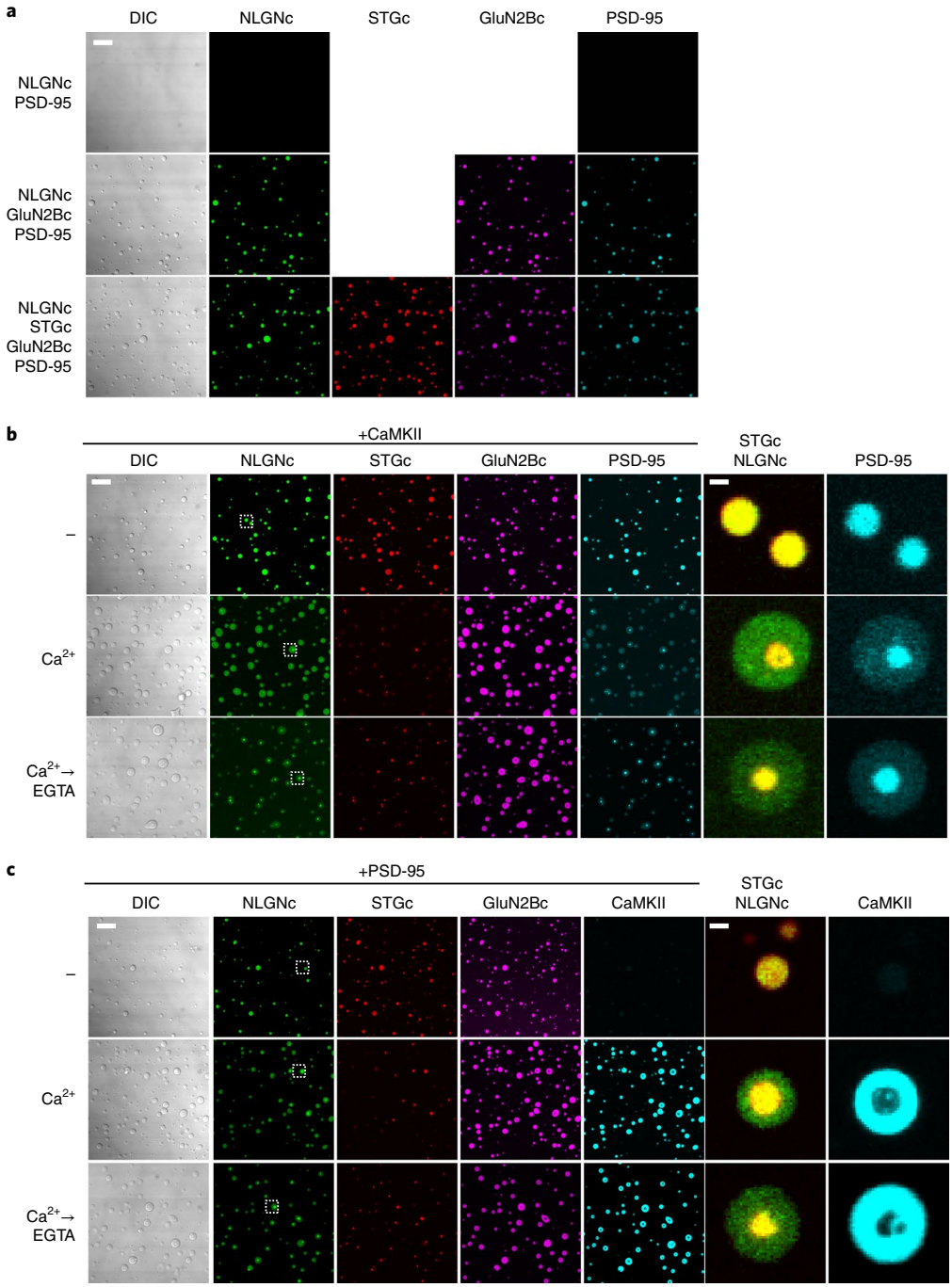

Fig. 5 | Neuroligin-1 segregates into the STGc/PSD-95 phase by CaMKII. a, Images of protein mixtures (as indicated). PSD-95 (10 μM) was mixed with 10 μM NLGNc (upper) and a further 10 μM GluN2Bc (middle) and 10 μM STGc (lower). No Ca^{2+} was added. NLGNc plus PSD-95 in the absence of GluN2Bc did not form condensate. This indicates that NLGNc participates in the condensates formed by PSD-95 and GluN2Bc as a 'client'. **b**, Condensates of 10 μM PSD-95, 2.5 μM GluN2Bc, 7.5 μM STGc, 1 μM NLGNc and unlabeled CaMKII in –, Ca^{2+} and Ca^{2+} → EGTA conditions. The right column shows a higher magnification image of condensates indicated by dashed rectangles in the NLGNc channel. Due to the limited number of color channels available, we used unlabeled CaMKII and labeled PSD-95. **c**, Same experiment as in **b** but using labeled CaMKII and unlabeled PSD-95. Scale bars, 10 μm and 1 μm for low- and high-magnification images, respectively. NLGNc/STGc segregate from CaMKII/GluN2Bc to form phase-in-phase while CaMKII and GluN2Bc are in the surrounding phase in the presence of Ca^{2+}. Once formed, the phase-in-phase organization remained, even after EGTA was added.

are surrounded by plasma membrane and have only a limited amount of proteins. Membrane proteins (receptors and cell adhesion molecules) are especially spatially limited because they exist two dimensionally at the synapse. Nevertheless, the result obtained in vitro shows that it is possible for CaMKII to undergo LLPS with its binding partners at the synapse.

In condensates, CaMKII segregated AMPAR and NMDAR into different compartments. Super-resolution imaging of the native AMPAR and NMDAR provided in vivo evidence that CaMKII segregates these two subtypes of glutamate receptor into different nanodomains (Supplementary Fig. 12a). AMPAR partitions together with NLGN and can form a link with the presynaptic active

zone. This mechanism may enrich AMPAR beneath the transmitter release site. AMPAR has a low affinity to glutamate compared with NMDAR and is normally not saturated with glutamate at the synaptic cleft[33–35]. Indeed, super-resolution imaging studies showed the alignment of pre- and postsynaptic markers, termed synaptic nanomodules or nanocolumns, is refined as a result of neuronal activation[5,6]. The segregation of AMPARs under the transmitter release site can increase the efficacy of synaptic transmission (Supplementary Fig. 12b)[24]. Furthermore, cluster formation of NLGN induces clustering of presynaptic neurexin, which then recruits further axonal vesicular release machinery and eventually forms an active zone[36]. Therefore, the postsynaptic clustering of NLGN may serve as a retrograde mechanism to increase presynaptic release probability (Supplementary Fig. 12b)[27]. Combining these processes, we propose that postsynaptic activation of CaMKII and resultant formation of LLPS can serve as a new modulatory mechanism of synaptic transmission. Consistent with this idea, the activation of postsynaptic NMDAR accumulates more active zone proteins over the postsynaptic PSD-95 cluster, thereby forming a trans-synaptically matched nanocolumn of release machinery and receptor complex at the synapse[5].

GluN2B is a minor component of PSD proteins[37] and the CaMKII T-site can interact with other proteins, such as Tiam1, GJD2/connexin 36, LRRC7/densin-180, Camk2n1 and L-type Ca^{2+} channel. Therefore, it is possible that CaMKII forms condensates with these proteins as well, although GluN2B is the most important partner for CaMKII[17]. Through this mechanism, CaMKII can serve as a postsynaptic Ca^{2+}-dependent hub, which underlies the activity-dependent transport and crosslinking of several postsynaptic client proteins observed during LTP via the LLPS-mediated mechanism[30,38]. This reasonably explains the dodecameric structure and abundance of CaMKII.

In conclusion, we found a new property of CaMKII in undergoing LLPS in Ca^{2+}-dependent manner and segregating different synaptic proteins. In the future, it will be crucial to test whether this mechanism works in situ and to determine the relative contribution of this versus other proposed mechanisms of synaptic plasticity mediated by CaMKII, such as AMPAR phosphorylation, insertion and translocation[39–41].

Online content

Any methods, additional references, Nature Research reporting summaries, source data, extended data, supplementary information, acknowledgements, peer review information; details of author contributions and competing interests; and statements of data and code availability are available at https://doi.org/10.1038/s41593-021-00843-3.

Received: 9 June 2020; Accepted: 22 March 2021;
Published online: 29 April 2021

References

1. Biederer, T., Kaeser, P. S. & Blanpied, T. A. Transcellular nanoalignment of synaptic function. *Neuron* **96**, 680–696 (2017).
2. Scheefhals, N. & MacGillavry, H. D. Functional organization of postsynaptic glutamate receptors. *Mol. Cell Neurosci.* **91**, 82–94 (2018).
3. Kellermayer, B. et al. Differential nanoscale topography and functional role of GluN2-NMDA receptor subtypes at glutamatergic synapses. *Neuron* **100**, 106–119 e107 (2018).
4. Goncalves, J. et al. Nanoscale co-organization and coactivation of AMPAR, NMDAR, and mGluR at excitatory synapses. *Proc. Natl Acad. Sci. USA* **117**, 14503–14511 (2020).
5. Tang, A. H. et al. A trans-synaptic nanocolumn aligns neurotransmitter release to receptors. *Nature* **536**, 210–214 (2016).
6. Hruska, M., Henderson, N., Le Marchand, S. J., Jafri, H. & Dalva, M. B. Synaptic nanomodules underlie the organization and plasticity of spine synapses. *Nat. Neurosci.* **21**, 671–682 (2018).
7. Hyman, A. A., Weber, C. A. & Julicher, F. Liquid–liquid phase separation in biology. *Annu. Rev. Cell Dev. Biol.* **30**, 39–58 (2014).
8. Chen, X., Wu, X., Wu, H. & Zhang, M. Phase separation at the synapse. *Nat. Neurosci.* **23**, 301–310 (2020).
9. Bayer, K. U., De Koninck, P., Leonard, A. S., Hell, J. W. & Schulman, H. Interaction with the NMDA receptor locks CaMKII in an active conformation. *Nature* **411**, 801–805 (2001).
10. Saneyoshi, T. et al. Reciprocal activation within a Kinase-Effector complex underlying persistence of structural LTP. *Neuron* **102**, 1199–1210 e1196 (2019).
11. Chao, L. H. et al. A mechanism for tunable autoinhibition in the structure of a human Ca^{2+}/calmodulin-dependent kinase II holoenzyme. *Cell* **146**, 732–745 (2011).
12. Hayashi, M. K. et al. The postsynaptic density proteins Homer and Shank form a polymeric network structure. *Cell* **137**, 159–171 (2009).
13. Zeng, M. et al. Reconstituted postsynaptic density as a molecular platform for understanding synapse formation and plasticity. *Cell* **174**, 1172–1187 e1116 (2018).
14. Zeng, M. et al. Phase transition in postsynaptic densities underlies formation of synaptic complexes and synaptic plasticity. *Cell* **166**, 1163–1175 e1112 (2016).
15. Lee, S. J., Escobedo-Lozoya, Y., Szatmari, E. M. & Yasuda, R. Activation of CaMKII in single dendritic spines during long-term potentiation. *Nature* **458**, 299–304 (2009).
16. Bayer, K. U. et al. Transition from reversible to persistent binding of CaMKII to postsynaptic sites and NR2B. *J. Neurosci.* **26**, 1164–1174 (2006).
17. Halt, A. R. et al. CaMKII binding to GluN2B is critical during memory consolidation. *EMBO J.* **31**, 1203–1216 (2012).
18. Ambadipudi, S., Biernat, J., Riedel, D., Mandelkow, E. & Zweckstetter, M. Liquid–liquid phase separation of the microtubule-binding repeats of the Alzheimer-related protein Tau. *Nat. Commun.* **8**, 275 (2017).
19. Nicoll, R. A., Tomita, S. & Bredt, D. S. Auxiliary subunits assist AMPA-type glutamate receptors. *Science* **311**, 1253–1256 (2006).
20. Zeng, M. et al. Phase separation-mediated TARP/MAGUK complex condensation and AMPA receptor synaptic transmission. *Neuron* **104**, 529–543 e526 (2019).
21. Lepicard, E. M., Mizuno, K., Antunes-Martins, A., von Hertzen, L. S. & Giese, K. P. An endogenous inhibitor of calcium/calmodulin-dependent kinase II is up-regulated during consolidation of fear memory. *Eur. J. Neurosci.* **23**, 3063–3070 (2006).
22. Vest, R. S., Davies, K. D., O'Leary, H., Port, J. D. & Bayer, K. U. Dual mechanism of a natural CaMKII inhibitor. *Mol. Biol. Cell* **18**, 5024–5033 (2007).
23. Trotter, J. H. et al. Synaptic neurexin-1 assembles into dynamically regulated active zone nanoclusters. *J. Cell Biol.* **218**, 2677–2698 (2019).
24. Xie, X., Liaw, J. S., Baudry, M. & Berger, T. W. Novel expression mechanism for synaptic potentiation: alignment of presynaptic release site and postsynaptic receptor. *Proc. Natl Acad. Sci. USA* **94**, 6983–6988 (1997).
25. Scheiffele, P., Fan, J., Choih, J., Fetter, R. & Serafini, T. Neuroligin expressed in nonneuronal cells triggers presynaptic development in contacting axons. *Cell* **101**, 657–669 (2000).
26. Haas, K. T. et al. Pre-post synaptic alignment through neuroligin-1 tunes synaptic transmission efficiency. *eLife* **7**, e31755 (2018).
27. Futai, K. et al. Retrograde modulation of presynaptic release probability through signaling mediated by PSD-95-neuroligin. *Nat. Neurosci.* **10**, 186–195 (2007).
28. Okamoto, K., Nagai, T., Miyawaki, A. & Hayashi, Y. Rapid and persistent modulation of actin dynamics regulates postsynaptic reorganization underlying bidirectional plasticity. *Nat. Neurosci.* **7**, 1104–1112 (2004).
29. Shen, K. & Meyer, T. Dynamic control of CaMKII translocation and localization in hippocampal neurons by NMDA receptor stimulation. *Science* **284**, 162–166 (1999).
30. Bosch, M. et al. Structural and molecular remodeling of dendritic spine substructures during long-term potentiation. *Neuron* **82**, 444–459 (2014).
31. Cai, Q. et al. CaMKIIα-driven, phosphatase-checked postsynaptic plasticity via phase separation. *Cell Res.* **31**, 37–51 (2020).
32. Takao, K. et al. Visualization of synaptic Ca^{2+}/calmodulin-dependent protein kinase II activity in living neurons. *J. Neurosci.* **25**, 3107–3112 (2005).
33. Patneau, D. K. & Mayer, M. L. Structure–activity relationships for amino acid transmitter candidates acting at N-methyl-D-aspartate and quisqualate receptors. *J. Neurosci.* **10**, 2385–2399 (1990).
34. Tong, G. & Jahr, C. E. Block of glutamate transporters potentiates postsynaptic excitation. *Neuron* **13**, 1195–1203 (1994).
35. Liu, G., Choi, S. & Tsien, R. W. Variability of neurotransmitter concentration and nonsaturation of postsynaptic AMPA receptors at synapses in hippocampal cultures and slices. *Neuron* **22**, 395–409 (1999).
36. Dean, C. et al. Neurexin mediates the assembly of presynaptic terminals. *Nat. Neurosci.* **6**, 708–716 (2003).
37. Sheng, M. & Hoogenraad, C. C. The postsynaptic architecture of excitatory synapses: a more quantitative view. *Annu. Rev. Biochem.* **76**, 823–847 (2007).
38. Hell, J. W. CaMKII: claiming center stage in postsynaptic function and organization. *Neuron* **81**, 249–265 (2014).

39. Hayashi, Y. et al. Driving AMPA receptors into synapses by LTP and CaMKII: requirement for GluR1 and PDZ domain interaction. *Science* **287**, 2262–2267 (2000).
40. Hosokawa, T., Mitsushima, D., Kaneko, R. & Hayashi, Y. Stoichiometry and phosphoisotypes of hippocampal AMPA type glutamate receptor phosphorylation. *Neuron* **85**, 60–67 (2015).
41. Diering, G. H. & Huganir, R. L. The AMPA receptor code of synaptic plasticity. *Neuron* **100**, 314–329 (2018).

Methods

Guidelines. All recombinant DNA and animal experiments were carried out in accordance with the institutional guidelines of Kyoto University, Hong Kong University of Science and Technology, University of Bordeaux and CNRS.

DNA constructs and protein purification. Rat CaMKII wildtype and mutants, fluorescent proteins fused with Spy-catcher, Spy-tag fused with the intracellular carboxyl tails of GluN2Bc (mouse, amino acids (a.a.) 1226–1482), STGc (mouse, a.a. 203–323), NLGNc (mouse, a.a. 719–843), GluA1 (rat, a.a. 827–907), and GluA2 (rat, a.a. 834–883) at their amino-termini were inserted into the vector pSUMO (ref. [42]). Amino acid residues were numbered with the initiation methionine as 1. PSD-95 and calmodulin were inserted into the p32m3c vector as previously described[13].

All proteins were expressed in *Escherichia coli* strain BL21 DE3 RIL and purified by affinity column using Nickel–NTA beads (Nacalai Tesque), gel filtration column HiLoad 26/600 Superdex 200 pg (GE Healthcare) and anion exchange column HiTrap Q HP (GE Healthcare). All tags for purification were cut and removed. The I205K mutant of CaMKII was tagged with green fluorescent protein (GFP) due to the difficulty of expressing and purifying untagged protein.

Fluorescent protein tagged Spy-catcher and Spy-tag tagged receptor C-tails[42] were mixed with excess molar ratio of monomer C-tails and incubated for 2 h at room temperature to covalently conjugate with each other. Extra monomer C-tails were removed by further gel filtration. PSD-95 and CaMKII was labeled by iFluor 405 succinimidyl ester or iFluor 488 succinimidyl ester (AAT Bioquest) as previously described[13]. Labeled protein was mixed with unlabeled protein at 1:100. Protein concentration is expressed as monomer concentration throughout the study.

Formation and observation of LLPS condensates. Proteins were mixed in a buffer containing 50 mM Tris–HCl pH 7.5, 100 mM NaCl, 1 mM Tris(2-carboxyethyl) phosphine (TCEP), 0.5 mM EGTA and 10 μM calmodulin in the presence of 5 mM $MgCl_2$ and 2.5 mM ATP (− condition). $MgCl_2$ and ATP were not added in Fig. 1f and Supplementary Fig. 6b. $CaCl_2$ (2 mM) was added to activate CaMKII (Ca^{2+} condition) and, 10 s later, 2.5 mM EGTA was further added to chelate Ca^{2+} (Ca^{2+} → EGTA condition) to mimic a transient Ca^{2+} signal.

The sedimentation assay was carried out as previously described[12–14]. The protein sample in a low protein binding tube (WATSON) was centrifuged at 10,000*g* for 1 min. Pellet and supernatant was denatured by SDS loading buffer and adjusted to the same volume. Samples (5 μl) were loaded onto SDS–polyacrylamide gel electrophoresis (SDS–PAGE) and visualized using Coomassie brilliant blue dye.

For confocal microscope imaging, a sample chamber was made between a coverslip (12 mm round coverslip, MATSUNAMI) and a slide glass (FRC-04, MATSUNAMI) separated by double-sided adhesive paper tape as a spacer. Protein mixture (5 μl) was injected into this space and the condensates were allowed to settle to the bottom of coverslip for 5 min. Observation was by a confocal microscopy system (FLUOVIEW FV1200, Olympus). The observation area was determined randomly. Images of each color channel were obtained with excitation wavelength and bandpass filters as follows: 405 nm for iFluor-405-tagged PSD-95 or CaMKII, 488 nm for iFluor-488-tagged CaMKII or Kusabira Green-tagged NLGNc, 546 nm for DsRed2-tagged STGc and 647 nm for eqFP670-tagged GluN2Bc and E2-Crimson-tagged GluA1c and GluA2c. Tiam1 peptide (mouse, a.a. 1540–1560) was labeled with fluorescein by N-hydroxysuccinimide (NHS)-ester at the amino terminus.

Turbidity assay. CaMKII (10 μM) and GluN2Bc (10 μM) were mixed in buffer containing 50 mM Tris–HCl pH 7.5, 100 mM NaCl, 1 mM Tris(2-carboxyethyl) phosphine (TCEP), 0.5 mM EGTA and 10 μM calmodulin in the presence of 5 mM $MgCl_2$ and 2.5 mM ATP. The turbidity of the protein sample was measured as the optical density at 420 nm by nanodrop ND-1000 (Thermo Fisher). The baseline was defined as zero, and the turbidity was measured every 30 s for 4 min. $CaCl_2$ (2 μM) was added at between 1 and 1.5 min, and 2.5 mM EGTA was further added between 2.5 and 3 min.

Cell culture, drug treatment and immunostaining. Banker-type cultures of hippocampal neurons were prepared from embryonic day 18 (E18) Sprague–Dawley rats of both sexes at a density of 200,000 cells per dish as described[4,43]. The neurons at 16 days in vitro were treated with the CaMKII inhibitor peptide CN21 fused with the cell-penetrating peptide TAT (TAT-CN21; YGRKKRRQRRRKRPPKLGQIGRSKRVVIEDDR) or a scrambled CN21 with TAT (TAT-scrambled; YGRKKRRQRRRVKEPRIDGKPVRLRGQKSDRI) (20 μM) for 30 min. After treatment, the neurons were surface-immunolabeled for endogenous glutamate receptor labeling: GluA2 (anti-GluA2, clone 14B11, 0.0033 μg μl^{-1}. IgG2b; provided by E. Gouaux) and GluN1 (anti-GluN1, clone 10B11, 0.002 μg μl^{-1}. IgG1; provided by E. Gouaux) at 37 °C for 15 min (refs. [4,43]). Neuroligin-1 was labeled with biotin by coexpressing acceptor peptide (AP)-tagged neuroligin-1 and a biotin ligase BirA (ref. [44]). The cells were surface labeled by incubating with monovalent streptavidin coupled to Alexa 647 for 10 min. After three washes, the cells were fixed with 4% paraformaldehyde (Sigma-Aldrich, catalog no. P6148)/4% sucrose (Sigma-Aldrich, catalog no. 0389) in phosphate buffered saline (PBS) at room temperature for 10 min and treated with blocking solution (1.5% bovine serum albumin (Sigma-Aldrich, catalog no. A3059)/0.1% fish skin gelatin/0.1% Triton X-100 in PBS/NH_4Cl) at room temperature for 1 h. Cells were then incubated with secondary antibodies, goat anti-mouse IgG2b Alexa 647 (Thermo Scientific, catalog no. 21242. 0.002 μg μl^{-1}) and goat anti-mouse IgG1 Alexa 532 (Thermo Scientific, and coupling done at IINS. 0.002 μg μl^{-1}) at room temperature for 1 h. Following three washes, a second fixation was performed and cells were then imaged.

dSTORM imaging. dSTORM imaging was performed on a LEICA DMi8 microscope equipped with a Leica HCX PL APO ×160 1.43 NA oil immersion TIRF objective and fiber-coupled laser launch (532 nm and 642 nm) (Roper Scientific). Single fluorophores were detected with an EMCCD camera (Evolve Photometrics). Samples were mounted on a Ludin chamber (Life Imaging Services) and 600 μl dSTORM pyranose switching buffer[45] was added. An extra coverslip was placed on top to minimize buffer evaporation and oxygen exchanges with ambient air. Before dSTORM imaging, a diffraction limited image of the target region (512 × 512 pixels, 1 pixel = 100 nm) was taken under wide-field epifluorescence illumination. Image acquisition was steered by MetaMorph software (Molecular Devices) with a 30 ms exposure time, 20,000 frames per color. The 642 nm and 532 nm lasers were used sequentially. Multicolor fluorescent microspheres (Tetraspeck, Invitrogen, catalog no. T7279) were used as fiducial markers for nanometer scale lateral drift correction and dual color registration.

Nanodomain analyses. To analyze AMPAR and NMDAR nanodomains, intensity super-resolution images with a pixel size of 25 nm were reconstructed during the acquisition using WaveTracer software operating as a plugin of MetaMorph[46]. Lateral drifts were corrected automatically from the localizations of fluorescent fiduciary markers absorbed into the coverslip. Single-molecule localizations of Alexa 532 and Alexa 647 were aligned postacquisition with PALMTracer software using a third-order polynomial transform to correct for chromatic aberrations on the whole field of view. SR-Tesseler and Coloc-Tesseler tessellation-based analysis software[47,48] were used to quantify the nanodomains and the colocalization of AMPAR and NMDAR, respectively. The segmentation of AMPAR and NMDAR nanodomains was performed separately. Single-molecule localizations were used to compute the Voronoï tessellation, from which the first rank order local density map was computed. Clusters were segmented automatically using a threshold of twice the average local density of the whole dataset, with a minimum localizations number of five and a minimum area of 2×10^4 nm^2. Next, the clusters' nanodomains were segmented by applying a threshold of one times the average density in each cluster, with a minimum localizations number of 25, a minimum area 0.02 (AMPAR) or 0.01 (NMDAR) $\times 10^4$ nm^2. The colocalization between AMPAR and NMDAR was computed from the overlapping nanodomains area in selected regions of interest (ROI). ROIs were identified from merged epifluorescence images of AMPAR and NMDAR.

NLGN1 and NMDAR double-stained images were analyzed similarly but, because they hardly overlapped, we measured the distance from NMDAR localization to the nearest NLGN1 localization with a cut-off of 500 nm. Statistical significance was tested by Kolmogorov–Smirnov test; α was set at 0.05.

Statistics and reproducibility. No animals/datapoints were excluded. No statistical methods were used to predetermine sample sizes but our sample sizes are similar to those reported in previous publications[4,43]. We used GraphPad Prism Software v.8.3.1 to perform statistical analysis. The normality and equal variances of datasets were tested, and suitable statistical tests were chosen according to the datasets. Two-sided Mann–Whitney *U* was used for Fig. 4 and Supplementary Fig. 8 and Kolmogorov–Smirnov test was used for Supplementary Fig. 11. The reproducibility of all micrographs shown in this paper was confirmed in more than four independent experiments.

Reporting Summary. Further information on research design is available in the Nature Research Reporting Summary linked to this article.

Data availability

All relevant data of this manuscript are available from the corresponding author upon reasonable request. Protein sequences are available from NCBI (https://www.ncbi.nlm.nih.gov/protein/).

References

42. Zakeri, B. et al. Peptide tag forming a rapid covalent bond to a protein, through engineering a bacterial adhesin. *Proc. Natl Acad. Sci. USA* **109**, E690–E697 (2012).
43. Nair, D. et al. Super-resolution imaging reveals that AMPA receptors inside synapses are dynamically organized in nanodomains regulated by PSD95. *J. Neurosci.* **33**, 13204–13224 (2013).
44. Chamma, I. et al. Mapping the dynamics and nanoscale organization of synaptic adhesion proteins using monomeric streptavidin. *Nat. Commun.* **7**, 10773 (2016).

45. Beghin, A. et al. Localization-based super-resolution imaging meets high-content screening. *Nat. Methods* **14**, 1184–1190 (2017).
46. Kechkar, A., Nair, D., Heilemann, M., Choquet, D. & Sibarita, J. B. Real-time analysis and visualization for single-molecule based super-resolution microscopy. *PLoS One* **8**, e62918 (2013).
47. Levet, F. et al. SR-Tesseler: a method to segment and quantify localization-based super-resolution microscopy data. *Nat. Methods* **12**, 1065–1071 (2015).
48. Levet, F. et al. A tessellation-based colocalization analysis approach for single-molecule localization microscopy. *Nat. Commun.* **10**, 2379 (2019).

Acknowledgements

We thank R. A. Nicoll, J. W. Hell and T. A. Blanpied for comments on the manuscript, E. Gouaux, O. Thoumine, M. Sainlos, M. Rosendale and Bordeaux Imaging Center for the reagents and assistance and L. Yu, A. Z. Weitemier and E. Agnello for editing. This work was supported by RIKEN Presidents Fund, SPIRITS 2019 of Kyoto University, Grant-in-Aid for Scientific Research JP20240032, JP22110006, JP16H01292, JP18H04733 and JP18H05434 from the MEXT, Japan, JST, CREST JPMJCR20E4, Japan, Programme Exploration France from Ambassade de France au Japon, The Uehara Memorial Foundation, The Naito Foundation, Research Foundation for Opto-Science and Technology, Novartis Foundation, The Takeda Science Foundation and Japan Foundation for Applied Enzymology to Y.H., The Takeda Science Foundation and Grants-in-Aid for Scientific Research JP17K14947, JP18KK0421 and JP19K06885 from the MEXT, Japan to T.H., grants from the Simons Foundation (Award ID 510178) and Research Grant Council of Hong Kong (AoE-M09-12 and C6004-17G) to M.Z., HFSP Research Grant (RGP0020/2019) jointly to Y.H. and M.Z, CRCNS-NIH-ANR AMPAR-T fellowship to E.H. and The National Center for Scientific Research (CNRS), Agence Nationale de la Recherche (DynHippo) to L.G. and J.F.

Author contributions

T.H. and P.-W.L. conducted and managed all experiments. Y.H. managed the overall project. Q.C. and M.Z. participated in LLPS experiments. J.S.F., F.L., C.B., J.-B.S., D.C., L.G. and E.H. participated in super-resolution microscopy.

Competing interests

Y.H. is partly supported by Fujitsu Laboratories and Dwango.

Additional information

Supplementary information The online version contains supplementary material available at https://doi.org/10.1038/s41593-021-00843-3.

Correspondence and requests for materials should be addressed to M.Z. or Y.H.

Peer review information *Nature Neuroscience* thanks Thomas Biederer, Dragomir Milovanovic and the other, anonymous, reviewer(s) for their contribution to the peer review of this work.

Reprints and permissions information is available at www.nature.com/reprints.

nature research

Corresponding author(s): Yasunori Hayashi

Last updated by author(s): Feb 7, 2021

Reporting Summary

Nature Research wishes to improve the reproducibility of the work that we publish. This form provides structure for consistency and transparency in reporting. For further information on Nature Research policies, see our Editorial Policies and the Editorial Policy Checklist.

Statistics

For all statistical analyses, confirm that the following items are present in the figure legend, table legend, main text, or Methods section.

n/a	Confirmed	
☐	☒	The exact sample size (*n*) for each experimental group/condition, given as a discrete number and unit of measurement
☐	☒	A statement on whether measurements were taken from distinct samples or whether the same sample was measured repeatedly
☐	☒	The statistical test(s) used AND whether they are one- or two-sided *Only common tests should be described solely by name; describe more complex techniques in the Methods section.*
☒	☐	A description of all covariates tested
☒	☐	A description of any assumptions or corrections, such as tests of normality and adjustment for multiple comparisons
☒	☐	A full description of the statistical parameters including central tendency (e.g. means) or other basic estimates (e.g. regression coefficient) AND variation (e.g. standard deviation) or associated estimates of uncertainty (e.g. confidence intervals)
☐	☒	For null hypothesis testing, the test statistic (e.g. *F*, *t*, *r*) with confidence intervals, effect sizes, degrees of freedom and *P* value noted *Give P values as exact values whenever suitable.*
☒	☐	For Bayesian analysis, information on the choice of priors and Markov chain Monte Carlo settings
☒	☐	For hierarchical and complex designs, identification of the appropriate level for tests and full reporting of outcomes
☒	☐	Estimates of effect sizes (e.g. Cohen's *d*, Pearson's *r*), indicating how they were calculated

Our web collection on statistics for biologists contains articles on many of the points above.

Software and code

Policy information about availability of computer code

Data collection	Fluoview from Olympus, MetaMorph
Data analysis	ImageJ, MetaMorph, WaveTracer,SR-Tesseler and Coloc-Tesseler, PALMTracer

For manuscripts utilizing custom algorithms or software that are central to the research but not yet described in published literature, software must be made available to editors and reviewers. We strongly encourage code deposition in a community repository (e.g. GitHub). See the Nature Research guidelines for submitting code & software for further information.

Data

Policy information about availability of data

All manuscripts must include a data availability statement. This statement should provide the following information, where applicable:

- Accession codes, unique identifiers, or web links for publicly available datasets
- A list of figures that have associated raw data
- A description of any restrictions on data availability

All data generated or analyzed during this study are included in this article.

Field-specific reporting

Please select the one below that is the best fit for your research. If you are not sure, read the appropriate sections before making your selection.

☒ Life sciences ☐ Behavioural & social sciences ☐ Ecological, evolutionary & environmental sciences

For a reference copy of the document with all sections, see nature.com/documents/nr-reporting-summary-flat.pdf

Life sciences study design

All studies must disclose on these points even when the disclosure is negative.

Sample size	No statistical methods were used to pre-determine sample sizes but our sample sizes are similar to those reported in previous publications
Data exclusions	No animals/data points were excluded.
Replication	The reproducibility of all micrographs shown in this paper was confirmed by more than four times independent experiments.
Randomization	The observation area of micrographs was randomly determined
Blinding	All neurons were processed in parallel using the same staining, acquisition and analysis parameters in blind fashion.

Behavioural & social sciences study design

All studies must disclose on these points even when the disclosure is negative.

Study description	*Briefly describe the study type including whether data are quantitative, qualitative, or mixed-methods (e.g. qualitative cross-sectional, quantitative experimental, mixed-methods case study).*
Research sample	*State the research sample (e.g. Harvard university undergraduates, villagers in rural India) and provide relevant demographic information (e.g. age, sex) and indicate whether the sample is representative. Provide a rationale for the study sample chosen. For studies involving existing datasets, please describe the dataset and source.*
Sampling strategy	*Describe the sampling procedure (e.g. random, snowball, stratified, convenience). Describe the statistical methods that were used to predetermine sample size OR if no sample-size calculation was performed, describe how sample sizes were chosen and provide a rationale for why these sample sizes are sufficient. For qualitative data, please indicate whether data saturation was considered, and what criteria were used to decide that no further sampling was needed.*
Data collection	*Provide details about the data collection procedure, including the instruments or devices used to record the data (e.g. pen and paper, computer, eye tracker, video or audio equipment) whether anyone was present besides the participant(s) and the researcher, and whether the researcher was blind to experimental condition and/or the study hypothesis during data collection.*
Timing	*Indicate the start and stop dates of data collection. If there is a gap between collection periods, state the dates for each sample cohort.*
Data exclusions	*If no data were excluded from the analyses, state so OR if data were excluded, provide the exact number of exclusions and the rationale behind them, indicating whether exclusion criteria were pre-established.*
Non-participation	*State how many participants dropped out/declined participation and the reason(s) given OR provide response rate OR state that no participants dropped out/declined participation.*
Randomization	*If participants were not allocated into experimental groups, state so OR describe how participants were allocated to groups, and if allocation was not random, describe how covariates were controlled.*

Ecological, evolutionary & environmental sciences study design

All studies must disclose on these points even when the disclosure is negative.

Study description	*Briefly describe the study. For quantitative data include treatment factors and interactions, design structure (e.g. factorial, nested, hierarchical), nature and number of experimental units and replicates.*
Research sample	*Describe the research sample (e.g. a group of tagged Passer domesticus, all Stenocereus thurberi within Organ Pipe Cactus National Monument), and provide a rationale for the sample choice. When relevant, describe the organism taxa, source, sex, age range and any manipulations. State what population the sample is meant to represent when applicable. For studies involving existing datasets, describe the data and its source.*

Sampling strategy	*Note the sampling procedure. Describe the statistical methods that were used to predetermine sample size OR if no sample-size calculation was performed, describe how sample sizes were chosen and provide a rationale for why these sample sizes are sufficient.*
Data collection	*Describe the data collection procedure, including who recorded the data and how.*
Timing and spatial scale	*Indicate the start and stop dates of data collection, noting the frequency and periodicity of sampling and providing a rationale for these choices. If there is a gap between collection periods, state the dates for each sample cohort. Specify the spatial scale from which the data are taken*
Data exclusions	*If no data were excluded from the analyses, state so OR if data were excluded, describe the exclusions and the rationale behind them, indicating whether exclusion criteria were pre-established.*
Reproducibility	*Describe the measures taken to verify the reproducibility of experimental findings. For each experiment, note whether any attempts to repeat the experiment failed OR state that all attempts to repeat the experiment were successful.*
Randomization	*Describe how samples/organisms/participants were allocated into groups. If allocation was not random, describe how covariates were controlled. If this is not relevant to your study, explain why.*
Blinding	*Describe the extent of blinding used during data acquisition and analysis. If blinding was not possible, describe why OR explain why blinding was not relevant to your study.*

Did the study involve field work? ☐ Yes ☐ No

Field work, collection and transport

Field conditions	*Describe the study conditions for field work, providing relevant parameters (e.g. temperature, rainfall).*
Location	*State the location of the sampling or experiment, providing relevant parameters (e.g. latitude and longitude, elevation, water depth).*
Access & import/export	*Describe the efforts you have made to access habitats and to collect and import/export your samples in a responsible manner and in compliance with local, national and international laws, noting any permits that were obtained (give the name of the issuing authority, the date of issue, and any identifying information).*
Disturbance	*Describe any disturbance caused by the study and how it was minimized.*

Reporting for specific materials, systems and methods

We require information from authors about some types of materials, experimental systems and methods used in many studies. Here, indicate whether each material, system or method listed is relevant to your study. If you are not sure if a list item applies to your research, read the appropriate section before selecting a response.

Materials & experimental systems

n/a	Involved in the study
☐	☒ Antibodies
☒	☐ Eukaryotic cell lines
☒	☐ Palaeontology and archaeology
☒	☐ Animals and other organisms
☒	☐ Human research participants
☒	☐ Clinical data
☒	☐ Dual use research of concern

Methods

n/a	Involved in the study
☒	☐ ChIP-seq
☒	☐ Flow cytometry
☒	☐ MRI-based neuroimaging

Antibodies

Antibodies used	anti-GluA2, clone 14B11, 0.0033 µg/µl. IgG2b. From Dr. Eric Gouaux, anti-GluN1, clone 10B11, 0.002 µg/µl. IgG1. From Dr. Gouaux
Validation	Anti-GluA2 antibodies used in this study gave no staining in GluA2 knockout mice (see also Giannone et al., Biophysical journal 99, 1303-1310). Specificity of anti-GluN1 was confirmed by FSEC traces in Lu et al., Science 2017 Mar 24; 355(6331)

Eukaryotic cell lines

Policy information about cell lines

Cell line source(s)	*State the source of each cell line used.*
Authentication	*Describe the authentication procedures for each cell line used OR declare that none of the cell lines used were authenticated.*

Mycoplasma contamination	*Confirm that all cell lines tested negative for mycoplasma contamination OR describe the results of the testing for mycoplasma contamination OR declare that the cell lines were not tested for mycoplasma contamination.*
Commonly misidentified lines (See ICLAC register)	*Name any commonly misidentified cell lines used in the study and provide a rationale for their use.*

Palaeontology and Archaeology

Specimen provenance	*Provide provenance information for specimens and describe permits that were obtained for the work (including the name of the issuing authority, the date of issue, and any identifying information).*
Specimen deposition	*Indicate where the specimens have been deposited to permit free access by other researchers.*
Dating methods	*If new dates are provided, describe how they were obtained (e.g. collection, storage, sample pretreatment and measurement), where they were obtained (i.e. lab name), the calibration program and the protocol for quality assurance OR state that no new dates are provided.*

☐ Tick this box to confirm that the raw and calibrated dates are available in the paper or in Supplementary Information.

Ethics oversight	*Identify the organization(s) that approved or provided guidance on the study protocol, OR state that no ethical approval or guidance was required and explain why not.*

Note that full information on the approval of the study protocol must also be provided in the manuscript.

Animals and other organisms

Policy information about studies involving animals; ARRIVE guidelines recommended for reporting animal research

Laboratory animals	*For laboratory animals, report species, strain, sex and age OR state that the study did not involve laboratory animals.*
Wild animals	*Provide details on animals observed in or captured in the field; report species, sex and age where possible. Describe how animals were caught and transported and what happened to captive animals after the study (if killed, explain why and describe method; if released, say where and when) OR state that the study did not involve wild animals.*
Field-collected samples	*For laboratory work with field-collected samples, describe all relevant parameters such as housing, maintenance, temperature, photoperiod and end-of-experiment protocol OR state that the study did not involve samples collected from the field.*
Ethics oversight	*Identify the organization(s) that approved or provided guidance on the study protocol, OR state that no ethical approval or guidance was required and explain why not.*

Note that full information on the approval of the study protocol must also be provided in the manuscript.

Human research participants

Policy information about studies involving human research participants

Population characteristics	*Describe the covariate-relevant population characteristics of the human research participants (e.g. age, gender, genotypic information, past and current diagnosis and treatment categories). If you filled out the behavioural & social sciences study design questions and have nothing to add here, write "See above."*
Recruitment	*Describe how participants were recruited. Outline any potential self-selection bias or other biases that may be present and how these are likely to impact results.*
Ethics oversight	*Identify the organization(s) that approved the study protocol.*

Note that full information on the approval of the study protocol must also be provided in the manuscript.

Clinical data

Policy information about clinical studies

All manuscripts should comply with the ICMJE guidelines for publication of clinical research and a completed CONSORT checklist must be included with all submissions.

Clinical trial registration	*Provide the trial registration number from ClinicalTrials.gov or an equivalent agency.*
Study protocol	*Note where the full trial protocol can be accessed OR if not available, explain why.*
Data collection	*Describe the settings and locales of data collection, noting the time periods of recruitment and data collection.*
Outcomes	*Describe how you pre-defined primary and secondary outcome measures and how you assessed these measures.*

Dual use research of concern

Policy information about dual use research of concern

Hazards

Could the accidental, deliberate or reckless misuse of agents or technologies generated in the work, or the application of information presented in the manuscript, pose a threat to:

No	Yes	
☐	☐	Public health
☐	☐	National security
☐	☐	Crops and/or livestock
☐	☐	Ecosystems
☐	☐	Any other significant area

Experiments of concern

Does the work involve any of these experiments of concern:

No	Yes	
☐	☐	Demonstrate how to render a vaccine ineffective
☐	☐	Confer resistance to therapeutically useful antibiotics or antiviral agents
☐	☐	Enhance the virulence of a pathogen or render a nonpathogen virulent
☐	☐	Increase transmissibility of a pathogen
☐	☐	Alter the host range of a pathogen
☐	☐	Enable evasion of diagnostic/detection modalities
☐	☐	Enable the weaponization of a biological agent or toxin
☐	☐	Any other potentially harmful combination of experiments and agents

ChIP-seq

Data deposition

☐ Confirm that both raw and final processed data have been deposited in a public database such as GEO.

☐ Confirm that you have deposited or provided access to graph files (e.g. BED files) for the called peaks.

Data access links *May remain private before publication.*	*For "Initial submission" or "Revised version" documents, provide reviewer access links. For your "Final submission" document, provide a link to the deposited data.*
Files in database submission	*Provide a list of all files available in the database submission.*
Genome browser session (e.g. UCSC)	*Provide a link to an anonymized genome browser session for "Initial submission" and "Revised version" documents only, to enable peer review. Write "no longer applicable" for "Final submission" documents.*

Methodology

Replicates	*Describe the experimental replicates, specifying number, type and replicate agreement.*
Sequencing depth	*Describe the sequencing depth for each experiment, providing the total number of reads, uniquely mapped reads, length of reads and whether they were paired- or single-end.*
Antibodies	*Describe the antibodies used for the ChIP-seq experiments; as applicable, provide supplier name, catalog number, clone name, and lot number.*
Peak calling parameters	*Specify the command line program and parameters used for read mapping and peak calling, including the ChIP, control and index files used.*
Data quality	*Describe the methods used to ensure data quality in full detail, including how many peaks are at FDR 5% and above 5-fold enrichment.*
Software	*Describe the software used to collect and analyze the ChIP-seq data. For custom code that has been deposited into a community repository, provide accession details.*

Flow Cytometry

Plots

Confirm that:

☐ The axis labels state the marker and fluorochrome used (e.g. CD4-FITC).

☐ The axis scales are clearly visible. Include numbers along axes only for bottom left plot of group (a 'group' is an analysis of identical markers).

☐ All plots are contour plots with outliers or pseudocolor plots.

☐ A numerical value for number of cells or percentage (with statistics) is provided.

Methodology

Sample preparation	*Describe the sample preparation, detailing the biological source of the cells and any tissue processing steps used.*
Instrument	*Identify the instrument used for data collection, specifying make and model number.*
Software	*Describe the software used to collect and analyze the flow cytometry data. For custom code that has been deposited into a community repository, provide accession details.*
Cell population abundance	*Describe the abundance of the relevant cell populations within post-sort fractions, providing details on the purity of the samples and how it was determined.*
Gating strategy	*Describe the gating strategy used for all relevant experiments, specifying the preliminary FSC/SSC gates of the starting cell population, indicating where boundaries between "positive" and "negative" staining cell populations are defined.*

☐ Tick this box to confirm that a figure exemplifying the gating strategy is provided in the Supplementary Information.

Magnetic resonance imaging

Experimental design

Design type	*Indicate task or resting state; event-related or block design.*
Design specifications	*Specify the number of blocks, trials or experimental units per session and/or subject, and specify the length of each trial or block (if trials are blocked) and interval between trials.*
Behavioral performance measures	*State number and/or type of variables recorded (e.g. correct button press, response time) and what statistics were used to establish that the subjects were performing the task as expected (e.g. mean, range, and/or standard deviation across subjects).*

Acquisition

Imaging type(s)	*Specify: functional, structural, diffusion, perfusion.*
Field strength	*Specify in Tesla*
Sequence & imaging parameters	*Specify the pulse sequence type (gradient echo, spin echo, etc.), imaging type (EPI, spiral, etc.), field of view, matrix size, slice thickness, orientation and TE/TR/flip angle.*
Area of acquisition	*State whether a whole brain scan was used OR define the area of acquisition, describing how the region was determined.*

Diffusion MRI ☐ Used ☐ Not used

Preprocessing

Preprocessing software	*Provide detail on software version and revision number and on specific parameters (model/functions, brain extraction, segmentation, smoothing kernel size, etc.).*
Normalization	*If data were normalized/standardized, describe the approach(es): specify linear or non-linear and define image types used for transformation OR indicate that data were not normalized and explain rationale for lack of normalization.*
Normalization template	*Describe the template used for normalization/transformation, specifying subject space or group standardized space (e.g. original Talairach, MNI305, ICBM152) OR indicate that the data were not normalized.*
Noise and artifact removal	*Describe your procedure(s) for artifact and structured noise removal, specifying motion parameters, tissue signals and physiological signals (heart rate, respiration).*

Volume censoring

Define your software and/or method and criteria for volume censoring, and state the extent of such censoring.

Statistical modeling & inference

Model type and settings

Specify type (mass univariate, multivariate, RSA, predictive, etc.) and describe essential details of the model at the first and second levels (e.g. fixed, random or mixed effects; drift or auto-correlation).

Effect(s) tested

Define precise effect in terms of the task or stimulus conditions instead of psychological concepts and indicate whether ANOVA or factorial designs were used.

Specify type of analysis: ☐ Whole brain ☐ ROI-based ☐ Both

Statistic type for inference
(See Eklund et al. 2016)

Specify voxel-wise or cluster-wise and report all relevant parameters for cluster-wise methods.

Correction

Describe the type of correction and how it is obtained for multiple comparisons (e.g. FWE, FDR, permutation or Monte Carlo).

Models & analysis

n/a	Involved in the study
☐	☐ Functional and/or effective connectivity
☐	☐ Graph analysis
☐	☐ Multivariate modeling or predictive analysis

Functional and/or effective connectivity

Report the measures of dependence used and the model details (e.g. Pearson correlation, partial correlation, mutual information).

Graph analysis

Report the dependent variable and connectivity measure, specifying weighted graph or binarized graph, subject- or group-level, and the global and/or node summaries used (e.g. clustering coefficient, efficiency, etc.).

Multivariate modeling and predictive analysis

Specify independent variables, features extraction and dimension reduction, model, training and evaluation metrics.